Microscopic anisotropy revealed by NMR double pulsed field gradient experiments with arbitrary timing parameters

Evren Özarslan[a] and Peter J. Basser
Section on Tissue Biophysics and Biomimetics, NICHD, National Institutes of Health, 13 South Drive, Bethesda, Maryland 20892, USA

(Received 1 February 2008; accepted 14 March 2008; published online 17 April 2008)

We consider a general double pulsed field gradient experiment with arbitrary experimental parameters and calculate an exact expression for the NMR signal attenuation from restricted geometries, which is valid at long wavelengths, i.e., when the product of the gyromagnetic ratio of the spins, the pulsed gradients' duration, and their magnitude is small compared to the reciprocal of the pore size. It is possible to observe microscopic anisotropy within the pore space induced by the boundaries of the pore, which can be used to differentiate restricted from free or multicompartmental diffusion and to estimate a characteristic pore dimension in the former case. Explicit solutions for diffusion taking place between parallel plates as well as in cylindrical and spherical pores are provided. In coherently packed cylindrical pores, it is possible to measure simultaneously the cylinders' orientation and diameter using small gradient strengths. The presence of orientational heterogeneity of cylinders is addressed, and a scheme for differentiating microscopic from ensemble anisotropy is proposed. [DOI: 10.1063/1.2905765]

I. INTRODUCTION

Diffusion of spin bearing molecules in porous media observably affects the nuclear magnetic resonance (NMR) signal. Inferring microstructural features of the pore from the diffusion NMR signal attenuation has proven to be of paramount value in a variety of applications from oil-well logging and dynamics of polymers to the diagnosis and monitoring of many diseases in the human body. The most commonly used NMR method with which to observe diffusion in porous media employs the pulsed field gradient (PFG) experiments,[1] where a pair of pulsed magnetic field gradients is applied to encode displacements between the application of these two pulses.

Although the PFG experiments have been useful in characterizing pore microstructure, many additional features, particularly those related to different length scales of porous media, can be gleaned if different pulse sequences are employed. One such alternative is the multi-PFG experiment, which involves the application of repeated pairs of diffusion gradients as proposed in Ref. 2. Variants of this pulse sequence have been considered for and found useful in various applications.[3–10] The simplest version of such sequences employs only two pairs of gradients; a spin-echo version of this double-PFG sequence is shown in Fig. 1(a). Here, each pulsed-gradient spin-echo (PGSE) block, comprising a pair of diffusion gradients of duration δ, sensitizes the signal to motion that occurs during an interval Δ. The movements of molecules during the two encoding intervals are correlated[11] when the mixing time t_m is finite. $\mathbf{G}_1$ and $\mathbf{G}_2$ denote the diffusion gradients of the first and second encoding blocks, respectively. Figure 1(b) shows another double-PGSE experiment, which results from the simultaneous application of the second and third gradients of the sequence in Fig. 1(a).

The acquisition and analysis schemes for double-PFG data depend on the structure to be examined. For example, in Ref. 12, the authors introduce a two-dimensional technique, where the strength of the first and second gradients is independently varied. When the diffusion process can be characterized locally by a diffusion tensor, then a two-dimensional Laplace transform can be employed to generate maps of diffusion coefficients depicting the correlations of motion during the two encoding periods. This approach has been applied to plant tissue,[13] as well as various phases of liquid crystals.[14–16]

The double-PFG experiments have received increasing attention recently due to the realization that such experiments are sensitive to restricted diffusion even at diffusion wavelengths that are long compared to the pore dimensions. Note that by diffusion wavelength we mean the quantity $\Lambda=(\gamma\delta G)^{-1}$, where γ denotes the gyromagnetic ratio of the spins and G is the gradient magnitude. The long diffusion wavelength regime ($\Lambda^2 \gg a^2$, where a is a characteristic pore size) is sometimes referred to as the small-q regime, $(2\pi qa)^2 \ll 1$, where q denotes the wave number, defined through the relationship $q=1/(2\pi\Lambda)=\gamma\delta G/(2\pi)$.

The sensitivity of the double-PFG experiments to restricted diffusion in this regime is a very desirable property, which makes it possible to probe small pores using relatively small diffusion gradient strengths. Recent findings[17–19] suggest that the dependence of the signal intensity on the angle between the two gradients, $\mathbf{G}_1$ and $\mathbf{G}_2$, may make it possible to determine the sizes of biological cells using moderate gradient strengths. Although such an angular dependence was predicted by Mitra,[4] his treatment considered only special limiting cases of the double-PFG experiment ($|\mathbf{G}_1|=|\mathbf{G}_2|$, Δ

[a]Electronic mail: evren@helix.nih.gov.

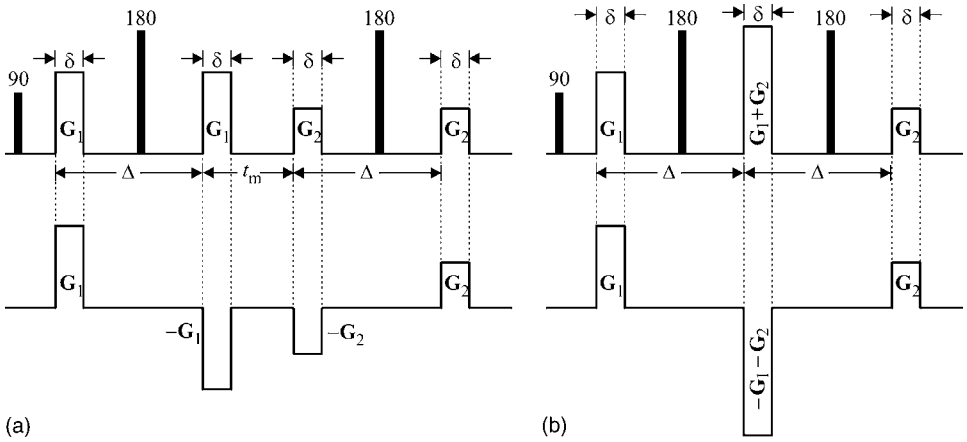

FIG. 1. (a) A general double-PGSE pulse sequence is shown on the top row. This pulse sequence features two distinct PGSE blocks separated from each other by the mixing time t_m. The pulse separation associated with each of the PGSE encodings is Δ, where each diffusion gradient is assumed to have the same pulse length δ. The resulting effective gradient waveform is shown on the bottom. (b) A similar experiment with the two middle gradients superposed. The mixing time is not defined for this pulse sequence.

$\rightarrow\infty$, $\delta=0$, and $t_m=0$ or $t_m\rightarrow\infty$), which are difficult to achieve in practice. Moreover, when even one of these conditions is not fully met, systematic errors in the estimations of the microstructural features are unavoidable. In this article, we provide solutions for the NMR signal intensity for arbitrary parameters of the double-PFG experiment, which is valid when the long diffusion wavelength condition, $(\gamma\delta Ga)^2\ll 1$, is met.

In a recent publication, we investigated the diffractionlike nonmonotonicity of the NMR signal in multi-PFG experiments.[9] Specifically, we showed that, when an even number of diffusion gradient pulse pairs is used, the NMR signal is expected to become negative at exactly half the wave number necessary to observe the nonmonotonicity in single-PFG experiments.[20] Apart from the beneficial reduction of the necessary gradient strength, this zero-crossing also makes it possible to determine an average pore size even when the specimen under investigation contains pores with a broad distribution of sizes. Despite these advantages, the observation of diffractionlike features from small pores can still be difficult because of the strict requirement on the wave number. The treatment presented here may be useful in such cases.

II. FREE DIFFUSION

We shall start by considering free (Gaussian) diffusion. The exact form of the signal attenuation obtained via arbitrary gradient waveforms is given by the expression[21]

$$E^{\text{free}}=\exp\left(-\gamma^2 D_0\int_0^T dt\left|\int_0^t \mathbf{G}(t')dt'\right|^2\right), \tag{1}$$

where D_0 is the bulk diffusivity and $\mathbf{G}(t)$ is the effective time-dependent gradient waveform, which starts at $t=0$ and ends at $t=T$. Evaluating this expression for the effective pulse sequence of Fig. 1(a), we obtain

$$E_a^{\text{free}}=e^{-\gamma^2 D_0\delta^2(\Delta-\delta/3)(G_1^2+G_2^2)}, \tag{2}$$

where $G_1=|\mathbf{G}_1|$ and $G_2=|\mathbf{G}_2|$. Similarly, for the experiment of Fig. 1(b), we get

$$E_b^{\text{free}}=e^{-\gamma^2 D_0\delta^2[(\Delta-\delta/3)(G_1^2+G_2^2)-(\delta/3)G_1G_2\cos\psi]}, \tag{3}$$

where ψ is the angle between $\mathbf{G}_1$ and $\mathbf{G}_2$. The derivations of the signal attenuation expressions above is similar to the derivation of the well-known Stejskal-Tanner expression, which can be found in Ref. 21. In fact, when either G_1 or G_2 is set to zero in the expressions for both experiments, the signal attenuation is given by the Stejskal-Tanner relation as expected.

III. RESTRICTED DIFFUSION IN ISOTROPIC PORES

We have obtained an expression, similar to Eq. (1), valid for restricted diffusion taking place in D-dimensional isotropic pores with nonrelaxing walls. The derivation is based on the realization that a matrix product approach,[22] originally designed to compute numerically the NMR signal attenuations obtained using generalized gradient waveforms, along with a discretization scheme for it,[9] can be used as analytical tools. The details of this derivation can be found in the Appendix. Note that the geometries considered here are infinite parallel plates separated by a distance $2a$, and cylinders and spheres of radius a for the cases of $D=1,2$, and 3, respectively. Then the signal attenuation, for small values of $\gamma\delta Ga$, when the gradients are applied perpendicular to the restricting walls of the geometry, is given by

$$E^{\text{rest}}\simeq 1-2\gamma^2a^2\sum_{n=1}^{\infty}s_{Dn}\int_0^T dt e^{\omega_{Dn}t}\mathbf{G}(t)\cdot\mathbf{F}_{Dn}(t), \tag{4}$$

with the following definitions:

$$\mathbf{F}_{Dn}(t)=\int_t^T \mathbf{G}(t')e^{-\omega_{Dn}t'}dt', \tag{5}$$

$$s_{Dn}=\frac{1}{\alpha_{Dn}^2(\alpha_{Dn}^2-D+1)}, \tag{6}$$

where s_{Dn} satisfy the relationship

$$\sum_{n=1}^{\infty}s_{Dn}=\frac{1}{2(2+D)}, \tag{7}$$

and finally

$$\omega_{Dn}=\frac{\alpha_{Dn}^2D_0}{a^2}, \tag{8}$$

where $\alpha_{1n}=(n-1/2)\pi$, and α_{2n} and α_{3n} are, respectively, the roots of the derivatives of the first order Bessel and spherical

Bessel functions, i.e., they satisfy the expressions $J_1'(\alpha_{2n})=0$ and $j_1'(\alpha_{3n})=0$. The subscripts D will be dropped henceforth for brevity.

Evaluating Eq. (4) for the effective gradient waveforms of Fig. 1, we obtain

$$E_a^{\text{rest}} \simeq 1-(A(G_1^2+G_2^2)+BG_1G_2\cos\psi), \tag{9}$$

and

$$E_b^{\text{rest}} \simeq 1-(A(G_1^2+G_2^2)+B'G_1G_2\cos\psi), \tag{10}$$

with the definitions

$$A=2\gamma^2a^2\sum_{n=1}^{\infty}s_n \times\left[\frac{2\delta}{\omega_n}-\frac{1}{\omega_n^2}(2-2e^{-\omega_n\delta}+e^{-\omega_n(\Delta-\delta)}-2e^{-\omega_n\Delta} +e^{-\omega_n(\Delta+\delta)})\right], \tag{11}$$

$$B=2\gamma^2a^2\sum_{n=1}^{\infty}\frac{s_n}{\omega_n^2}(e^{-\omega_n(t_m-\delta)}-2e^{-\omega_nt_m}+e^{-\omega_n(t_m+\delta)} -2e^{-\omega_n(\Delta+t_m-\delta)}+4e^{-\omega_n(\Delta+t_m)}-2e^{-\omega_n(\Delta+t_m+\delta)} +e^{-\omega_n(2\Delta+t_m-\delta)}-2e^{-\omega_n(2\Delta+t_m)}+e^{-\omega_n(2\Delta+t_m+\delta)}), \tag{12}$$

and

$$B'=2\gamma^2a^2\sum_{n=1}^{\infty}s_n \times\left[\frac{2\delta}{\omega_n}-\frac{1}{\omega_n^2}(2-2e^{-\omega_n\delta}+2e^{-\omega_n(\Delta-\delta)}-4e^{-\omega_n\Delta} +2e^{-\omega_n(\Delta+\delta)}-e^{-\omega_n(2\Delta-\delta)} +2e^{-\omega_n2\Delta}-e^{-\omega_n(2\Delta+\delta)})\right]. \tag{13}$$

The long wavelength behavior of the NMR signal attenuation from the constant gradient spin-echo experiments for the same geometries has already been considered by Neuman.[23] The expressions in Eqs. (17), (18), and (20) of Neuman's article can be reproduced from our results by the substitutions $\Delta=\delta$ along with either $G_1=0$ or $G_2=0$. Signal attenuation due to diffusion inside spherical geometries observed via single-PFG experiments is provided in Ref. 24, which can be shown to be consistent with our expression through the substitutions $D=3$ and either $G_1=0$ or $G_2=0$. As mentioned in the Introduction, Mitra studied the quadratic term of the signal from double-PFG experiments when $\delta=0$, $\Delta\to\infty$, and $G_1=G_2$.[4] He demonstrated that, under these conditions, and by further assuming that the mixing times are long, the quadratic term has no angular dependence. Similarly, for the case $t_m=0$, the signal attenuation is proportional to $1+2\cos^2(\psi/2)$, or equivalently $2+\cos\psi$. Both of these findings are simply special cases of our results as well.

Comparing the signal attenuation expressions for free diffusion with those for restricted diffusion suggests several interesting distinctions. In the case of free diffusion, the signal attenuation is independent of the mixing time, which is not the case when restrictions are present. Second, the free diffusion signal decay for the pulse sequence of Fig. 1(b) suggests that the signal intensity depends on the angle between the gradient vectors, whereas the first pulse sequence leads to a signal decay, which is independent of the gradient directions. However, the angular dependence of the pulse sequence of Fig. 1(b), in the case of free diffusion, is merely an effect of the finite pulse duration, and as such it is not a fundamental feature of the double-PFG experiment in the case of free diffusion. This peculiar behavior is essentially due to the way "cross terms" play out when the two pulses overlap. Although it can be neglected when the $\delta\ll\Delta$ condition is met, it is significant when δ is close to Δ. For example, when $\delta=\Delta$, and taking $|\mathbf{G}_1|=|\mathbf{G}_2|$, the logarithm of the signal attenuation is proportional to $4-\cos\psi$. Note that the restricted diffusion signal decay has a similar angular dependence (though in the opposite sense) in both pulse sequences. Consequently, we will now consider only the pulse sequence illustrated in Fig. 1(a). In this case, an angular dependence of the signal intensity becomes a characteristic feature of restricted diffusion and in turn makes it possible to distinguish restricted diffusion from Gaussian diffusion by varying only the angle between the two gradient vectors.

We note that, as pointed out in Ref. 4 the same pulse sequence would lead to ψ-independent signal decays when the diffusion process is multi-Gaussian, which would occur when there are two distinct Gaussian compartments. Both restricted diffusion and multi-Gaussian processes may lead to similar echo attenuations when single-PFG experiments are performed.

Figure 2 shows the dependence of the signal from spherical pores on the angle between $\mathbf{G}_1$ and $\mathbf{G}_2$. As can be seen in Fig. 2(a), there is significant angular variation of the signal at short mixing times. This apparent anisotropy is a manifestation of the influence of the pore boundaries on the diffusing molecules, which becomes observable at short mixing times, i.e., when there is significant correlation in the movements of spins during the separate encoding periods. Panel (b) of the same figure illustrates the signal intensity with varying Δ values. It is clear that the angular dependence tends to disappear as Δ gets shorter. However, for small pores, i.e., when a is small, the long Δ requirement is easy to fulfill. Similar behavior is observed when the diffusion gradient pulse width (δ) gets longer as demonstrated in Fig. 2(c). Note that since we are primarily interested in the long wavelength behavior, i.e., the case of small $\gamma\delta Ga$, applying relatively short pulses is likely to be feasible. Finally, in the last panel of Fig. 2, we illustrate the angular variation in the NMR signal with different values for the gradient strength. From a theoretical point of view, smaller gradients are preferred to fulfill the $(\gamma\delta Ga)^2\ll 1$ condition, violation of which could make the higher order terms significant, potentially leading to a bias in the pore size estimates. However, Fig. 2(d) suggests that larger gradients will lead to sharper signal profiles. This is particularly desirable for accurate resolution of the angular variation when the signal-to-noise ratio (SNR)

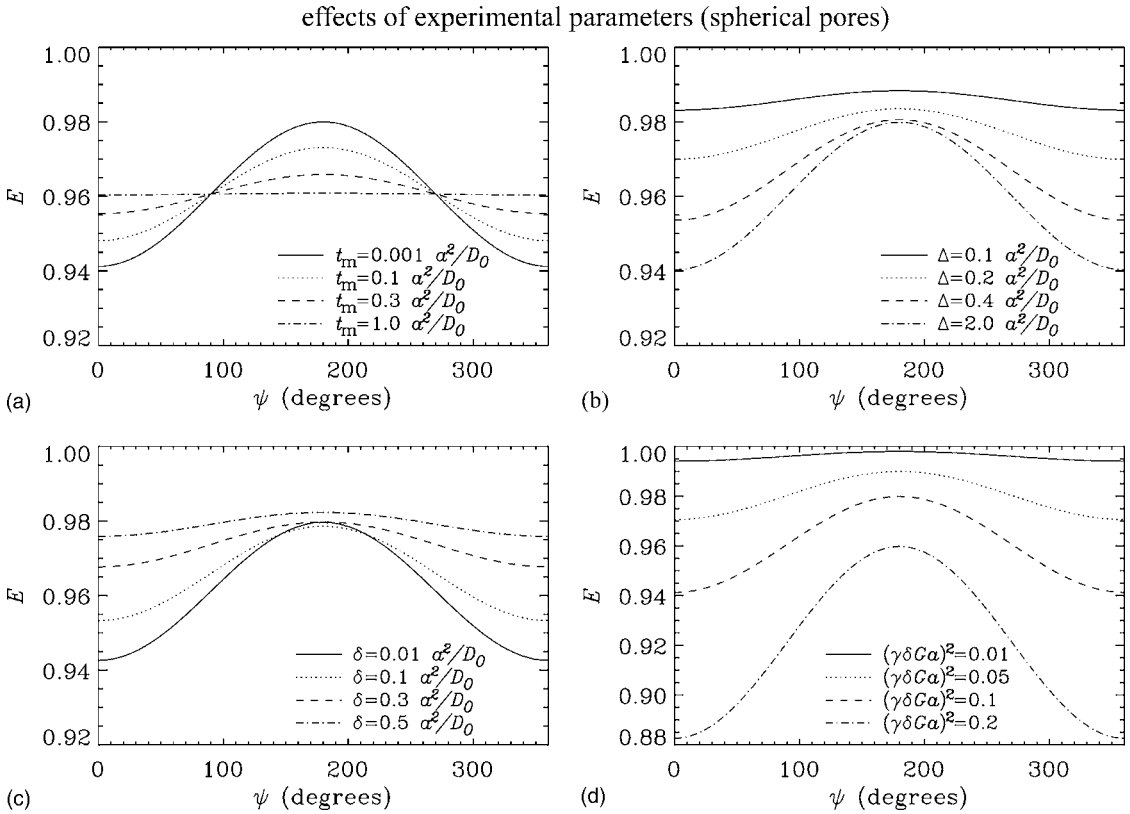

FIG. 2. Dependence of the NMR signal intensity from spherical pores on the angle between the gradients used in the two encoding blocks of a double-PFG experiment. The parameters used in the simulations were (a) $(\gamma\delta G_1 a)^2=(\gamma\delta G_2 a)^2=0.1$, $\delta=0.001a^2/D_0$, $\Delta=a^2/D_0$; (b) $(\gamma\delta G_1 a)^2=(\gamma\delta G_2 a)^2=0.1$, $\delta=0.001a^2/D_0$, $t_m=0.002a^2/D_0$; (c) $(\gamma\delta G_1 a)^2=(\gamma\delta G_2 a)^2=0.1$, $\Delta=a^2/D_0$, $t_m=0.002a^2/D_0$; and (d) $\delta=0.001a^2/D_0$, $\Delta=a^2/D_0$, $t_m=0.002a^2/D_0$.

is limited. Therefore, an optimal value for the gradient strength—which will depend on the SNR as well as the pore size—should exist.

In Fig. 3(a) we investigate the effects of variations in pore size within the specimen by averaging the signal attenuations from 10000 spheres whose radii are distributed according to a Rician distribution whose resulting mean and standard deviation values are denoted by a_0 and σ_a, respectively. Here, a Rician distribution is used to ensure that the radii will be positive even for relatively large values of σ_a. For each level of polydispersity, characterized by the σ_a value, we estimated an apparent pore size by fitting the signal values to the theoretical expression. The percentage errors were 0.00, 0.72, 1.6, and 2.5 for the cases of $\sigma_a=0$, $\sigma_a=0.2a$, $\sigma_a=0.3a$, and $\sigma_a=0.5a$, respectively. These findings suggest that the proposed method is robust to the heterogeneity of the specimen, making it possible to estimate an average pore size meaningfully by using double-PFG experiments.

To understand the robustness of the signal on polydispersity, in Fig. 3(b) we plot the signal for three values of ψ as a function of the pore size. Clearly, around the mean value of a_0, the signal curves are linear although some nonlinearity is visible when the gradients are in the opposite direction. Therefore, a pore size distribution, symmetric around the mean, with reasonably small standard deviations can be expected to yield accurate estimates of the average pore size as the effects of larger pores would be canceled by those due to small pores. However, most distributions of interest, like the Rician distributions we employed, are nonsymmetric. Therefore, the exact nature of the deviations in the pore size estimates from the mean pore size depends on the particular distribution as well as the dependence of the signal on pore size.

IV. DIFFUSION IN ANISOTROPIC PORES

Although we have provided results for isotropic pores, anisotropic environments can also be modeled using the same framework. For simplicity, we shall start by considering a specimen of coherently packed, infinitely long cylinders oriented along the direction $\mathbf{u}$. Then the gradient vectors $\mathbf{G}_1$ and $\mathbf{G}_2$ can be decomposed into components parallel and perpendicular to $\mathbf{u}$. This enables the evaluation of the signal intensity as a product of the signal attenuations from free diffusion and restricted diffusion with $D=2$

$$E_a^{\mathrm{cyl}}(\mathbf{u}) = E_a^{\mathrm{free}}(g_1,g_2) \times E_a^{\mathrm{rest}}(\mathbf{G}_1 - g_1\mathbf{u}, \mathbf{G}_2 - g_2\mathbf{u}), \quad (14)$$

where $g_i=\mathbf{G}_i\cdot\mathbf{u}$. The echo attenuation at long wavelengths is given by

$$E_a^{\mathrm{cyl}}(\mathbf{u}) \simeq e^{-\gamma^2 D_0 \delta^2(\Delta-\delta/3)(g_1^2+g_2^2)} \times (C + Ag_1^2 + Ag_2^2 + Bg_1g_2), \quad (15)$$

where

$$C = 1 - A(G_1^2 + G_2^2) - BG_1G_2\cos\psi. \quad (16)$$

In Fig. 4(b), we show the simulated signal attenuation when one of the gradients is applied along the direction perpendicular to the cylinder's surface as a function of the orientation of the second gradient. The geometry and gradient orientations are illustrated in Fig. 4(a). The θ dependence of each curve, when $\phi=90°$, is indicative of the ensemble anisotropy due to the coherence in the cylinders' orientations. The fact that different curves corresponding to different azimuthal angles (ϕ) do not coincide at $\theta=90°$ is a consequence of the microscopic anisotropy induced by restricted diffusion. Therefore, using double-PFG experiments, it is possible to probe ensemble (i.e., global) and microscopic anisotropy simultaneously. Note that while the orientation of the cylinders can be estimated using simple models like a diffusion tensor description of the quadratic term of the signal attenuation in a single-PFG experiment,[25] such a model would not account for restricted diffusion, making it impossible to estimate the diameters of the cylinders at long wavelengths.

A. General treatment of ensemble anisotropy

We shall now consider the case of variability in the cylinders' orientations. A general orientation distribution function $f(\mathbf{u})$ can be defined in terms of a Laplace series, i.e.,

$$f(\mathbf{u}) = \sum_{l=0,2,4,\ldots}^{\infty} \sum_{m=-l}^{l} f_{lm} Y_{lm}(\mathbf{u}), \tag{17}$$

where $Y_{lm}(\mathbf{u})$ are spherical harmonics. The resulting NMR signal attenuation is given by

$$E_a^{\mathrm{cyl}}(f(\mathbf{u})) = \sum_{l=0,2,4,\ldots}^{\infty} \sum_{m=-l}^{l} f_{lm} \times (CI_{lm}^{0,0} + AI_{lm}^{2,0} + AI_{lm}^{0,2} + BI_{lm}^{1,1}), \tag{18}$$

where $I_{lm}^{p,q}$ is given by the following integral over the sphere:

$$I_{lm}^{p,q} = \int_S d\mathbf{u} Y_{lm}(\mathbf{u}) g_1^p g_2^q e^{-\gamma^2 D_0 \delta^2 (\Delta - \delta/3)(g_1^2 + g_2^2)}. \tag{19}$$

Although the analytic evaluation of this integral is possible, it is quite tedious and the result involves many sums and Wigner matrices. Consequently, in our implementation, we adopted a numerical scheme and employed an iterated Gaussian quadrature algorithm with 96 transformation points.

Figure 4(c) shows the NMR signal attenuation when the cylinders have an angular dispersion, where the associated orientation distribution function is characterized by a second order Cartesian tensor whose largest eigenvalue is ten times its other two eigenvalues. The corresponding f_{lm} coefficients were computed using the relationships provided in Ref. 26. The principal eigenvector, i.e., the average orientation of the cylinders, was oriented along the z axis. Note that the simulations of Fig. 4(b) are just a special case of ensemble anisotropy when the orientation distribution function is a delta function. A comparison of panels (b) and (c) of Fig. 4 suggests that the angular dispersion of the cylinders leads to a substantial suppression of ensemble anisotropy as demonstrated by the flattening of the θ dependence. The ϕ dependence, however, is affected less significantly.

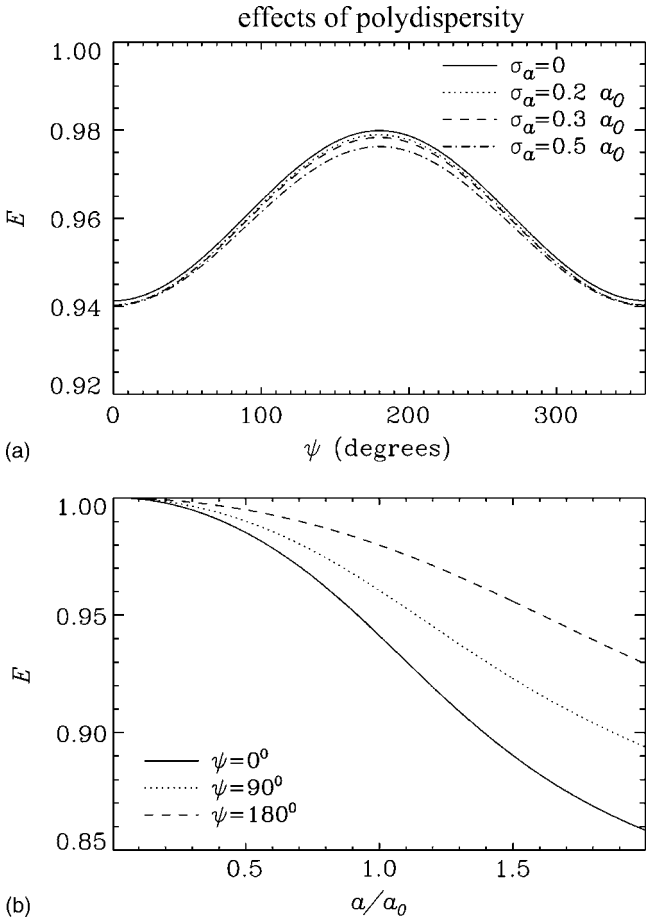

FIG. 3. In all simulations $(\gamma\delta G_1 a)^2=(\gamma\delta G_2 a)^2=0.1$, $t_m=0.002a^2/D_0$, $\Delta=a^2/D_0$, and $\delta=0.001a^2/D_0$. (a) Dependence of the NMR signal intensity from spherical pores on the angle between the gradients used in the two encoding blocks of a double-PFG experiment. The specimen was assumed to contain 10 000 spheres whose radii were distributed with a Rician distribution of mean value a_0 and standard deviation σ_a. (b) The dependence of the signal intensity from a single sphere on the radius of the sphere.

In Fig. 4(d), we show our simulation results from a bimodal orientation distribution function. This distribution was generated from an eight-order spherical tensor whose components, determined using the techniques in Ref. 27, will not be included for brevity. As the inset in Fig. 4(d) shows, two bundles of cylinders were used, whose average orientations are along the y and z axes. Note that the curves are qualitatively different from those of panels (b) and (c), suggesting the possibility of the resolution of fiber crossings using double-PFG experiments at long diffusion wavelengths.

Notably, when ϕ is equal to 90°, i.e., when $\mathbf{G}_2$ spans the plane of the distinct mean fiber orientations, the θ dependence of the signal almost disappears. To understand this insensitivity on θ when $\phi=90°$, we consider the case of two coherent and equally populated bundles, which are oriented along the y and z axes. Further assuming that $\gamma^2 D_0 \delta^2 (\Delta - \delta/3) G_2^2 \ll 1$, a straightforward application of Eq. (15) yields the expression

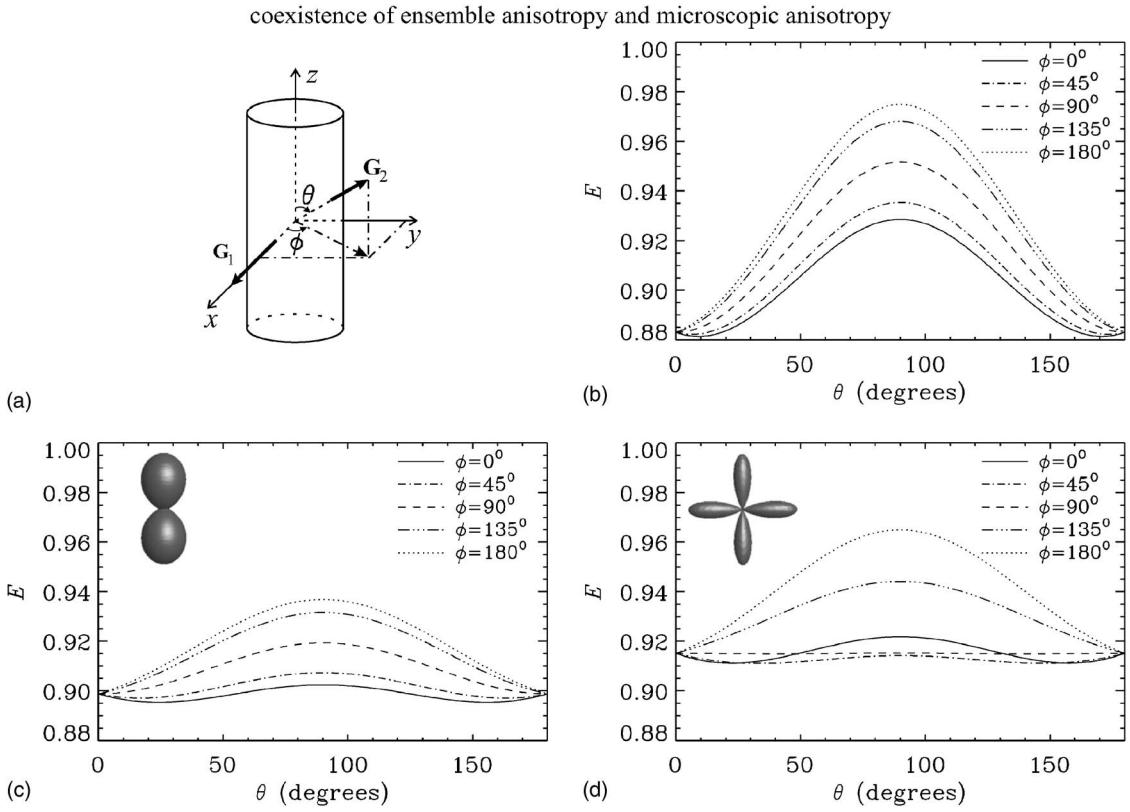

FIG. 4. In all simulations the following parameters were used: $\delta=0.001a^2/D_0$, $\Delta=a^2/D_0$, $t_m=0.002a^2/D_0$, and $(\gamma\delta G_1 a)^2=(\gamma\delta G_2 a)^2=0.1$. (a) The gradient orientations and the orientation of the cylinder, which is taken to be along the z axis. The direction of the first gradient is fixed along the x axis. The orientation of $\mathbf{G}_2$ is specified by the polar angle θ and the azimuthal angle ϕ. Note that with these definitions, the cosine of the angle between the two gradients is $\cos\psi=\sin\theta\cos\phi$. The NMR signal attenuation from (b) cylinders coherently oriented along the z axis, (c) cylinders with some angular dispersion where the mean orientation is along the z axis, and (d) cylinders with two distinct populations where the average orientation of one group is along the y axis, that of the other group is along the z axis. The surfaces displayed as insets in panels (c) and (d) illustrate the orientation distribution functions of the cylinders simulated.

$$E \simeq 1 - AG_1^2 - (A + \gamma^2 D_0 \delta^2(\Delta - \delta/3))\frac{G_2^2}{2} \tag{20}$$

for the signal attenuation, which is independent of θ. The very slight variation of the signal that we observed in Fig. 4(d) at $\phi=90°$ is due to the orientational incoherence within the individual bundles. Note that the above expression is valid only when the two fiber bundles are perpendicular to each other.

B. Isotropically distributed pores: A special case and a "component" of general distributions

Finally, we will discuss the case when all the fibers are isotropically distributed, which can be seen as a special case of the treatment of the previous subsection. However, because an irreducible representation of the orientation distribution function is employed, it can also be envisioned as the "isotropic component" of a possibly anisotropic orientation distribution. Therefore, the anisotropy predicted here can be attributed only to microscopic anisotropy even in the presence of ensemble anisotropy.

Note that regardless of the orientation distribution function, the first component of the spherical tensor representing it is given by $f_{00}=(4\pi)^{-1/2}$, which is a consequence of the normalization condition. In fact, this is the only nonzero coefficient when isotropic distributions are concerned. Therefore, the NMR signal attenuation is given by

$$E_a^{\mathrm{iso}}(f(\mathbf{u})) = \frac{1}{\sqrt{4\pi}}(CI_{00}^{0,0} + AI_{00}^{2,0} + AI_{00}^{0,2} + BI_{00}^{1,1}). \tag{21}$$

Since the integrand in the definition of $I_{00}^{p,q}$ is given in terms of dot products, it is rotationally invariant. Therefore, without loss of generality, the gradient vectors can be taken to be $\mathbf{G}_1^{\mathrm{T}}=G_1(1,0,0)$ and $\mathbf{G}_2^{\mathrm{T}}=G_2(\cos\psi,\sin\psi,0)$. This makes the evaluation of $I_{00}^{p,q}$ simple, which is given by

$$\begin{aligned} I_{00}^{p,q} = \sqrt{4\pi}\sum_{k=0}^{\infty}\sum_{r=0}^{k} & \times \frac{(-\gamma^2 D_0\delta^2(\Delta-\delta/3))^k}{(k-r)!r!}\frac{(2r+q)!}{(2k+p+q+1)!!} \\ & \times G_1^{2k-2r+p}G_2^{2r+q} \\ & \times \sum_{j=0,2,4\ldots}^{2r+q}\frac{(j-1)!!(2k+p+q-j-1)!!}{j!(2r+q-j)!} \\ & \times(\cos^{2r+q-j}\psi)(\sin^j\psi). \end{aligned} \tag{22}$$

Figure 5(a) shows the NMR signal attenuation from isotropically distributed cylinders. As pointed out above, only one mechanism of anisotropy influences the quadratic term, i.e., anisotropy due to microscopic restrictions. The angular variation of the signal is less than that predicted for coherently oriented cylinders. It is also meaningful to compare

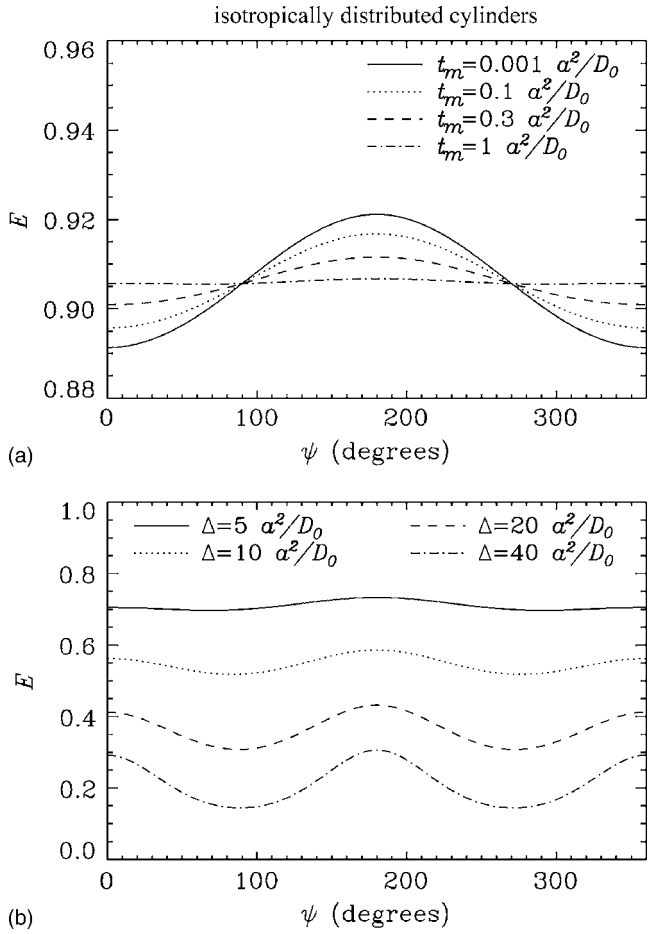

FIG. 5. NMR signal attenuation from cylinders isotropically distributed in space, obtained using a double-PFG experiment. In both simulations, the following parameters were used: $(\gamma\delta G_1 a)^2=(\gamma\delta G_2 a)^2=0.1$ and $\delta=0.001a^2/D_0$. (a) NMR signal attenuation with varying values of mixing time, where $\Delta=a^2/D_0$. (b) NMR signal attenuation with varying values of Δ, where $t_m=0.002a^2/D_0$.

these plots with Fig. 2(a), which shows the signal intensity with identical experimental parameters from spherical pores—another specimen that possesses only microscopic anisotropy. Qualitatively, the behavior is identical. However, because the molecules within isotropically distributed cylinders are not fully restricted, they suffer more signal loss.

1. Angular signal profile at very long diffusion times

Unlike the case of spherical pores, the loss of signal from isotropically distributed cylinders can be enhanced significantly by increasing the diffusion time. As depicted in Fig. 5(b), at very long diffusion times, the signal when the two gradients are approximately parallel decreases less and eventually approaches the case of antiparallel gradients—consistent with the case of infinitesimally small a as reported in Ref. 4.

In this section, we will elaborate on this qualitatively different angular dependence predicted for very large values of Δ. For this purpose, we consider a special yet instructive case of the experiment, where the following conditions are met: $t_m=\delta\rightarrow 0$, $G=G_1=G_2$, $T_0=D_0\Delta/a^2\gg 1$, $\kappa=\gamma\delta Ga\ll 1$, and define the dimensionless constant $\zeta=\gamma^2\delta^2G^2D_0\Delta=\kappa^2T_0$. Note that ζ can assume any value as it is the product of a small quantity (κ^2) and a large quantity (T_0). In fact, our goal in this section is to describe the behavior of the angular signal profile when one moves from the $\zeta\leqslant 1$ to $\zeta\gg 1$ regime.

When the above conditions are met, the attenuations due to restricted and free diffusion are given by the relations

$$E_a^{\mathrm{rest}}(\mathbf{u})=1-\frac{\gamma^2\delta^2a^2}{4}(|\mathbf{G}_{1\perp}|^2+|\mathbf{G}_{2\perp}|^2+\mathbf{G}_{1\perp}\cdot\mathbf{G}_{2\perp}), \tag{23a}$$

$$E_a^{\mathrm{free}}(\mathbf{u})=e^{-\gamma^2\delta^2D_0\Delta(g_1^2+g_2^2)}, \tag{23b}$$

where $\mathbf{G}_{i\perp}=\mathbf{G}_i-g_i\mathbf{u}$ is the component of the ith gradient ($i=1,2$) perpendicular to the cylinder's axis. Note that in the above expressions we are considering the signal from a single tube whose axis is specified by the unit vector $\mathbf{u}$ whose polar and azimuthal coordinates will be denoted by θ and ϕ, respectively.

We first consider the cases $\psi=0$ and $\psi=\pi$. Because the dot products of $\mathbf{G}_1$ with $\mathbf{G}_2$ are given by $+G^2$ and $-G^2$, we will refer to these two cases by the superscripts "+" and "−," respectively. Since the cylinders are isotropically distributed, without loss of generality, the first diffusion gradient can be taken to be along the z direction, i.e., $\mathbf{G}_1=G\mathbf{z}$. Then $\mathbf{G}_2^{\pm}=\pm G\mathbf{z}$. It is straightforward to show that $g_1=\pm g_2^{\pm}=G\cos\theta$, $\mathbf{G}_{1\perp}=\pm\mathbf{G}_{2\perp}^{\pm}$, and $|\mathbf{G}_{1\perp}|=|\mathbf{G}_{2\perp}^{\pm}|=G\sin\theta$. These lead to a simple expression for the signal attenuation from a single cylinder given by

$$E_a^{\pm}(\theta,\phi)=e^{-2\zeta\cos^2\theta}\left(1-\frac{\xi^{\pm}\kappa^2}{4}\sin^2\theta\right), \tag{24}$$

where $\xi^+=3$ and $\xi^-=1$. Averaging over all cylinder orientations yields

$$E_a^{\pm}=\int_0^1 e^{-2\zeta\mu^2}\left[1-\frac{\xi^{\pm}\kappa^2}{4}(1-\mu^2)\right]d\mu. \tag{25}$$

Next, we consider the case of $\psi=90°$, which will be denoted by the superscript "⊥." Similar to the cases in the preceding paragraph, without loss of generality, we can take the two gradient vectors to be $\mathbf{G}_1=G\mathbf{x}$ and $\mathbf{G}_2=G\mathbf{y}$. It can be shown that $g_1=G\sin\theta\cos\phi$, $g_2=G\sin\theta\sin\phi$, $|\mathbf{G}_{1\perp}|^2=G^2(1-\sin^2\theta\cos^2\phi)$, $|\mathbf{G}_{2\perp}|^2=G^2(1-\sin^2\theta\sin^2\phi)$, and $\mathbf{G}_{1\perp}\cdot\mathbf{G}_{2\perp}=-G^2\sin^2\theta\sin\phi\cos\phi$. Using Eqs. (23a) and (23b), the signal attenuation from a single tube is given by

$$E_a^{\perp}(\theta,\phi)=e^{-\zeta\sin^2\theta}\times\left[1-\frac{\kappa^2}{4}(2-\sin^2\theta(1+\sin\phi\cos\phi))\right]. \tag{26}$$

This equation can be integrated over the sphere to yield

$$E_a^{\perp}=\int_0^1 e^{-\zeta(1-\mu^2)}\left[1-\frac{\kappa^2}{4}(1+\mu^2)\right]d\mu. \tag{27}$$

Although Eqs. (25) and (27) can be evaluated analytically, the results are not included as we can infer the desired information directly from these equations. Note that in these

equations, the exponential terms are due to free diffusion along the tubes' orientations while the factors in square brackets are due to restricted diffusion. Because of the $\kappa^2 \ll 1$ condition, the effect of restricted diffusion on the differences between the resulting signal attenuations corresponding to the three different ψ values considered is limited. When the diffusion time is not very long so that ζ is small, the effect of free diffusion can be neglected. However, as ζ is increased, the differences due to free diffusion attenuation become more and more significant, eventually making the differences due to terms in square brackets negligible. Since the free diffusion expressions are identical in the $\psi=0$ and $\psi=180°$ cases, as the value of ζ is increased, we start seeing similar values for E_a^+ and E_a^-. However, note that the free diffusion factor in Eq. (27) is different from the one in Eq. (25), giving rise to the more rapid collapse of the signal as ζ is increased at $\psi=90°$.

These results are not surprising considering that when the diffusion time is very long so that ζ is large, those cylinders whose orientation vectors have a significant component along either of the two diffusion gradients do not contribute to the aggregate signal significantly. Since more of the tubes will be in this situation when $\psi=90°$, the corresponding signal is lower than the signal at $\psi=0°$ or $\psi=180°$.

V. DISCUSSION

The form of the NMR signal attenuation given in Eq. (4) can be used to understand the effects of restricted diffusion in any NMR imaging and spectroscopy pulse sequence that employs gradients that are small enough—a requirement which is common to standard sequences but also desirable when one is interested in characterizing geometric features of small pores or in biological and clinical applications. In this work, we focused on the double-PFG experiments only.

We would like to stress that, using the solutions presented above, an apparent or average pore dimension can be estimated even when the pores are not perfectly spherical or cylindrical. If the diffusion time is long enough for the molecules to travel across the longest distance present in the pore and if the pores are randomly oriented, it is appropriate to use the solutions for spherical pores. Otherwise, the results obtained for distribution of cylinders can be expected to yield more meaningful results.

Many different experimental designs are possible for the analysis of double-PFG acquisitions and estimation of a pore size from them. In all our figures, we plotted the NMR signal attenuation versus angle curves. Estimation of a pore size is possible by directly fitting the relevant expression to such a single angular profile. However, when the SNR is limited, one may have to apply gradients that do not adequately satisfy the $(\gamma\delta Ga)^2 \ll 1$ condition to be able to resolve the angular variation of the signal. The same problem may occur when the size of the pores turns out to be larger than predicted before the acquisition. To alleviate any bias that may be introduced by the higher order terms in this case, data with multiple values of gradient strengths can be acquired. Then the slope of the $(\ln E)$ versus G^2 curve at the origin can be estimated (e.g., by fitting a fourth order polynomial, $x_0G^2+x_1G^3+x_2G^4$, to the data) along each angle. The resulting profile of slopes can be used in the estimation of a compartment size.

The small $\gamma\delta Ga$ regime considered here is the same one used in Mitra's work.[4] The ability to probe restricted diffusion in this regime is desirable in characterizing features of small pores. However, note that among other conditions, Mitra's results assume infinitesimally short gradient pulses. This assumption alone demands strong gradient strengths when very small pores are to be examined, because the signal should attenuate by an observable amount, i.e., $\gamma\delta Ga$ cannot be extremely small due to a finite SNR. However, our formulations do not assume such extreme values for any gradient timings. This ability furthers the feasibility of our approach by incorporating the duration of the gradient pulses, reducing the requirement for large gradient magnitudes.

Note that Figs. 2(a)–2(c), 5(a), and 5(b) all indicate that deviations from the idealized values for the timing parameters assumed in Mitra's work lead to significant deviations from his formulas. Therefore, our formulations are expected to improve the accuracy of the estimations. Furthermore, because our approach provides the possibility of performing the experiments with arbitrary timing parameters, it may be possible to design experiments with much greater flexibility and increase the dimensionality of the parameter space that can be spanned in diffusion NMR acquisitions while alleviating the stringent hardware requirements inherent in the PFG experiment.

Anisotropy induced by restricting boundaries[28] was exploited recently to estimate the orientations perpendicular to the walls of macroscopic pores in single-PFG imaging studies where the voxels are smaller than the pore size.[29] Anisotropy predicted in the double-PFG experiments can be envisioned to arise from the same phenomenon at a much smaller length scale.

Note that different length scales can be probed by varying the diffusion time in single-PFG experiments, as was done to quantify scaling laws in disordered media.[30] Clearly, the double-PFG method provides an alternative means to probe multiple length scales, and is capable of elucidating any local order that may be present. In fact, the coexistence of ensemble anisotropy along with microscopic anisotropy, as treated in this article, is an example of how double-PFG can be used to observe phenomena manifested in different length scales.

It is clear from our simulations that by observing the dependence of the NMR signal intensity on the angle between the gradients used in the two separate blocks of the double-PFG experiment, restricted diffusion can be observed and distinguished from free or multicompartmental Gaussian diffusion. Note that the origins of the upward curvature of the single-PFG NMR signal decay versus q^2 [i.e., $E(q^2)$] curves on semilogarithmic plots observed from tissue samples is a widely debated topic among the biological NMR community. The ability of the double-PFG experiments to discriminate multicompartmental from restricted diffusion is expected to further our understanding of the determinants of such behavior.

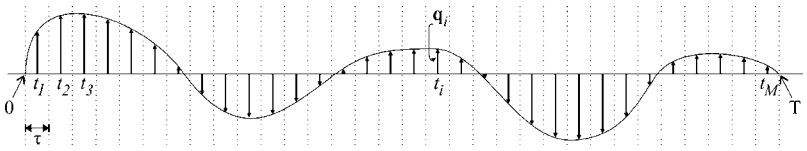

FIG. 6. The continuous line depicts a general NMR gradient waveform. An approximation is achieved by dividing the time axis into M intervals each of which contains an impulse. Note that the above waveform depicts the effective gradients, i.e., it is formed by taking into account the possible application of radiofrequency pulses.

VI. CONCLUSION

We have presented solutions for a general problem allowing many variations in experimental parameters as well as in the specimen under investigation. Our formalism started with a general expression (derived in the Appendix) that enables the evaluation of the effect of restricted diffusion at long wavelengths. We focused our attention on double-PFG experiments although similar analyses can be performed on a myriad of pulse sequences. We presented explicit solutions for diffusion taking place between infinite parallel plates as well as in cylindrical and spherical pores. The dependence of the signal intensity on the angle between the two gradients of the double-PFG experiments can be interpreted as a signature of local anisotropy induced by microscopic restrictions. Because the signal is also sensitive to ensemble anisotropy, which may be due to a coherence in the orientations of anisotropic pores, it was necessary to extract a term that included only microscopic anisotropy. This dependence was shown to be identical for anisotropic pores with perfectly isotropic orientation distributions. Our results can be used to design experiments with many degrees of parameters and to obtain accurate information on pore microstructure from double-PFG acquisitions, including compartment size and fiber orientation distributions—all from the long wavelength regime (i.e., the small-q behavior) of the NMR signal attenuation.

ACKNOWLEDGMENTS

We would like to thank Dr. Michal E. Komlosh for stimulating discussions and Liz Salak for editing the manuscript. This research was supported by the intramural research program of NICHD.

APPENDIX: THE DERIVATION OF THE NMR SIGNAL ATTENUATION FROM RESTRICTED GEOMETRIES AT LONG DIFFUSION WAVELENGTHS

The diffusion propagator $P(\mathbf{r},\mathbf{r}',t)$ denotes the displacement probability from the location $\mathbf{r}$ to $\mathbf{r}'$ during a time interval t and is the solution to the diffusion equation

$$D_0\nabla'^2 P(\mathbf{r},\mathbf{r}',t) = \frac{\partial P}{\partial t}, \tag{A1}$$

subject to the initial condition $P(\mathbf{r},\mathbf{r}',0)=\delta(\mathbf{r}-\mathbf{r}')$ and the boundary condition $\hat{\mathbf{n}}\cdot\nabla P\,(\mathbf{r},\mathbf{r}',t)|_{\mathbf{r}\in\Sigma}=0$ in pores with nonrelaxing impermeable walls, where $\hat{\mathbf{n}}$ is the direction perpendicular to the interface Σ at location $\mathbf{r}$. A convenient representation of the diffusion propagator is given by

$$P(\mathbf{r},\mathbf{r}',t) = \sum_{n=0}^{\infty} e^{-\lambda_n t} u_n(\mathbf{r}) u_n^*(\mathbf{r}'), \tag{A2}$$

where $u_n(\mathbf{r})$ is an eigenfunction of the Laplacian operator with the eigenvalue $-\lambda_n/D_0$. The long diffusion-time asymptotics of the propagator requires one of the eigenvalues to be 0. If this eigenvalue is denoted with index 0, then $u_0(\mathbf{r}) = V^{-1/2}$, where V is the pore volume.

In this Appendix, we consider a general gradient waveform as shown in Fig. 6. As proposed in Ref. 31, the gradient profile can be approximated by a train of impulses. We adopt the discretization suggested in Ref. 9, where the time axis is divided into M intervals of duration τ and the ith impulse $(1\leqslant i\leqslant M)$ is assumed to be applied at time t_i—the middle point of its respective interval. Then the magnitude of the impulse in the ith interval is taken to be

$$\mathbf{q}_i = \frac{\gamma}{2\pi}\int_{t_i-\tau/2}^{t_i+\tau/2} \mathbf{G}(t)dt, \tag{A3}$$

where γ is the gyromagnetic ratio of the spins, and $\mathbf{G}(t)$ is the time-dependent effective gradient waveform.

It was shown that using the eigenfunction expansion of the propagator as in Eq. (A2), the NMR signal attenuation can be expressed as a matrix product[22]

$$\tilde{E} = \mathbf{S}^T(\mathbf{q}_1)\mathbf{R}(\tau)\mathbf{A}(\mathbf{q}_2)\mathbf{R}(\tau)\mathbf{A}(\mathbf{q}_3)\mathbf{R}(\tau)\cdots \times\mathbf{R}(\tau)\mathbf{A}(\mathbf{q}_{M-1})\mathbf{R}(\tau)\mathbf{S}^*(-\mathbf{q}_M). \tag{A4}$$

Note that $\tilde{E}$ is an approximation to the true NMR signal attenuation, denoted by E, where any discrepancy between the two is due to the "time-slicing" employed in the construction of the matrix product scheme. Our approach to deriving a general expression for the signal attenuation involves evaluating $\tilde{E}$, and subsequently, taking the limit of the resulting expression as $\tau\to 0$, $M\to\infty$, while $M\tau=T$, similar to what is done in path integral (functional integration) methods.

In Eq. (A4), $\mathbf{S}$ is an M-dimensional vector whose kth component is given by the following integral over the pore volume V:

$$S_k(\mathbf{q}) = V^{-1/2}\int_V u_k(\mathbf{r})e^{i2\pi\mathbf{q}\cdot\mathbf{r}}d\mathbf{r}. \tag{A5}$$

Throughout this Appendix, the left subscript c in an expression ${}_cX(q)$ will denote the term proportional to $(2\pi qa)^c$ in a Taylor series expansion of the quantity X around $q=0$, where a is a characteristic length in the pore space. With this convention, it is straightforward to show that the vector $\mathbf{S}$ satisfies the relationships

$${}_cS_k(-\mathbf{q}) = (-1)^c\,{}_cS_k(\mathbf{q}), \tag{A6a}$$

$$ {}_0S_k(\mathbf{q}) = \delta_{0k}. \tag{A6b}$$

Similarly, $\mathbf{A}$ is an $M \times M$ matrix with components

$$ A_{km}(\mathbf{q}) = \int_V u_k^*(\mathbf{r}) u_m(\mathbf{r}) e^{i2\pi \mathbf{q}\cdot\mathbf{r}} d\mathbf{r}. \tag{A7}$$

Clearly, $\mathbf{A}$ satisfies the useful relationships

$$ \mathbf{A}(-\mathbf{q}) = \mathbf{A}^\dagger(\mathbf{q}), \tag{A8a}$$

$$ A_{0m}(\mathbf{q}) = S_m(\mathbf{q}), \tag{A8b}$$

$$ A_{k0}(\mathbf{q}) = S_k^*(-\mathbf{q}), \tag{A8c}$$

$$ {}_0A_{km}(\mathbf{q}) = \delta_{km}. \tag{A8d}$$

Finally, $\mathbf{R}$ is an $M \times M$ diagonal matrix with components

$$ R_{km}(t) = e^{-\lambda_k t}\delta_{km}, \tag{A9}$$

where the first element of $\mathbf{R}$ is unity, i.e., $R_{00}=1$. Note that both $\mathbf{A}$ and $\mathbf{R}$ satisfy the semigroup property, i.e.,

$$ \mathbf{A}(\mathbf{q}_1)\mathbf{A}(\mathbf{q}_2) = \mathbf{A}(\mathbf{q}_1 + \mathbf{q}_2), \tag{A10a}$$

$$ \mathbf{R}(t_1)\mathbf{R}(t_2) = \mathbf{R}(t_1 + t_2). \tag{A10b}$$

We are primarily interested in evaluating the signal attenuation value given in Eq. (A4) up to the terms of order $(4\pi^2 M^2 |\mathbf{q}_i||\mathbf{q}_j| a^2)$. For this purpose, the following relationships

$$ {}_0\mathbf{A}(\mathbf{q}_a)\mathbf{R}(t)\,{}_c\mathbf{S}^*(\mathbf{q}_b) = \mathbf{R}(t)\,{}_c\mathbf{S}^*(\mathbf{q}_b), \tag{A11a}$$

$$ {}_c\mathbf{S}^T(\mathbf{q}_a)\mathbf{R}(t)\,{}_0\mathbf{A}(\mathbf{q}_b) = {}_c\mathbf{S}^T(\mathbf{q}_a)\mathbf{R}(t), \tag{A11b}$$

$$ {}_c\mathbf{A}(\mathbf{q}_a)\mathbf{R}(t)\,{}_0\mathbf{S}^*(\mathbf{q}_b) = {}_c\mathbf{S}^*(-\mathbf{q}_a), \tag{A11c}$$

$$ {}_0\mathbf{S}^T(\mathbf{q}_a)\mathbf{R}(t)\,{}_c\mathbf{A}(\mathbf{q}_b) = {}_c\mathbf{S}^T(\mathbf{q}_b) \tag{A11d}$$

are helpful in simplifying the form of the matrix product in Eq. (A4). The zeroth order term of E is given by

$$ {}_0E = {}_0\mathbf{S}^T(\mathbf{q}_1)\mathbf{R}((M-1)\tau)\,{}_0\mathbf{S}^*(-\mathbf{q}_M) = 1. \tag{A12}$$

The expression

$$ {}_0\mathbf{S}^T(\mathbf{q}_a)\mathbf{R}(t)\,{}_1\mathbf{S}^*(\mathbf{q}_b) = -i\frac{2\pi}{V}\mathbf{q}_b\cdot\mathbf{r}_{\mathrm{cm}} \tag{A13}$$

is useful in evaluating the first order term given by

$$ {}_1\tilde{E} = i\frac{2\pi}{V}\mathbf{r}_{\mathrm{cm}}\cdot\sum_{j=1}^{M}\mathbf{q}_j. \tag{A14}$$

Inserting Eq. (A3) into the above expression yields

$$ {}_1E = i\frac{\gamma}{V}\mathbf{r}_{\mathrm{cm}}\cdot\int_0^T \mathbf{G}(t)dt, \tag{A15}$$

where $\mathbf{r}_{\mathrm{cm}}$ is the center-of-mass of the pore. When the integral above vanishes at the echo time, no contribution to the NMR signal is expected from the first order term.

For the second order term of the echo attenuation, one needs the quantities

$$ e_{20} = {}_2\mathbf{S}^T(\mathbf{q}_a)\mathbf{R}(t)\,{}_0\mathbf{S}^*(\mathbf{q}_b) = -\frac{2\pi^2}{V}\int_V (\mathbf{q}_a\cdot\mathbf{r})^2 d\mathbf{r}, \tag{A16}$$

and

$$ e_{11} = {}_1\mathbf{S}^T(\mathbf{q}_a)\mathbf{R}(t)\,{}_1\mathbf{S}^*(\mathbf{q}_b) = \frac{4\pi^2}{V}\int_V d\mathbf{r}\mathbf{q}_a\cdot\mathbf{r}\int_V d\mathbf{r}'\mathbf{q}_b\cdot\mathbf{r}' P(\mathbf{r},\mathbf{r}',t). \tag{A17}$$

The exact forms of e_{20} and e_{11} depend on the particular shape of the pore under consideration. Many pores of interest can be taken to be approximately isotropic. In fact, the pores commonly treated in the literature,[9,32] i.e., parallel plates and cylindrical and spherical pores, are simply isotropic pores in one, two, and three dimensions, respectively. If we take the radii of the cylindrical and spherical pores to be a and the separation between the two infinite plates to be $2a$, then the above integrals can be given by the unified expressions

$$ e_{20} = -\frac{2\pi^2 q_a^2 a^2}{(2+D)}, \tag{A18}$$

and

$$ e_{11} = 8\pi^2 a^2 \mathbf{q}_a\cdot\mathbf{q}_b\sum_{n=1}^{\infty} s_{Dn} e^{-\omega_{Dn}(t_b - t_a)}. \tag{A19}$$

Here, D is the dimension of the isotropic pore, and

$$ \omega_{Dn} = \frac{\alpha_{Dn}^2 D_0}{a^2}, \tag{A20}$$

where $\alpha_{1n}=(n-1/2)\pi$, and α_{2n} and α_{3n} satisfy the expressions $J_1'(\alpha_{2n})=0$ and $j_1'(\alpha_{3n})=0$, respectively. Here, $J_1(x)$ is the first order Bessel function and $j_1(x)$ is the first order spherical Bessel function.

The quantity s_{Dn} is given by

$$ s_{Dn} = \frac{1}{\alpha_{Dn}^2(\alpha_{Dn}^2 - D + 1)}. \tag{A21}$$

Note that s_{Dn} satisfy the relationship

$$ \sum_{n=1}^{\infty} s_{Dn} = \frac{1}{2(2+D)}, \tag{A22}$$

which can be established using Laplace transform techniques, or more simply by writing down the matrix product representation of the NMR signal (up to the quadratic term) for a single-PFG experiment in the narrow pulse regime and setting its $\Delta\to 0$ limit to 1.

These results can be combined to yield the following convenient form for the quadratic term of the NMR signal attenuation for a generalized gradient waveform:

$$ {}_2\tilde{E} = -4\pi^2 a^2 \sum_{j=1}^{M}\sum_{k=1}^{M}\mathbf{q}_j\cdot\mathbf{q}_k\sum_{n=1}^{\infty} s_{Dn} e^{-\omega_{Dn}|t_k - t_j|}. \tag{A23}$$

Inserting Eq. (A3) into the above expression twice and taking the $\tau\to 0$ limit yields

$$_2E = -2\gamma^2 a^2 \sum_{n=1}^{\infty} s_{Dn} \int_0^T dt e^{\omega_{Dn} t} \mathbf{G}(t) \cdot \mathbf{F}_{Dn}(t), \tag{A24}$$

where

$$\mathbf{F}_{Dn}(t) = \int_t^T \mathbf{G}(t') e^{-\omega_{Dn} t'} dt'. \tag{A25}$$

Therefore, the NMR signal at long diffusion wavelengths can be written as $E \simeq {}_0E + {}_1E + {}_2E$, where the terms in this expression are provided in Eqs. (A12), (A15), and (A24). When the integral of the effective gradient waveform vanishes, as is the case in both versions of the double-PFG experiment considered in this article, the first order term is zero and the NMR signal attenuation is given by Eq. (4).

This derivation demonstrates that the matrix product formalism developed by Callaghan,[22] along with the discretization scheme in Ref. 9, can be used as analytical tools for the derivation of NMR signal intensity obtained using generalized gradient waveforms.

[1] E. O. Stejskal and J. E. Tanner, J. Chem. Phys. **42**, 288 (1965).
[2] D. G. Cory, A. N. Garroway, and J. B. Miller, Polym. Prepr. (Am. Chem. Soc. Div. Polym. Chem.) **31**, 149 (1990).
[3] P. T. Callaghan and B. Manz, J. Magn. Reson., Ser. A **106**, 260 (1994).
[4] P. P. Mitra, Phys. Rev. B **51**, 15074 (1995).
[5] Y. Cheng and D. G. Cory, J. Am. Chem. Soc. **121**, 7935 (1999).
[6] J. Stepišnik and P. T. Callaghan, Physica B **292**, 296 (2000).
[7] S. Stapf, S.-I. Han, C. Heine, and B. Blümich, Concepts Magn. Reson. **14**, 172 (2002).
[8] P. T. Callaghan and M. E. Komlosh, Magn. Reson. Chem. **40**, S15 (2002).
[9] E. Özarslan and P. J. Basser, J. Magn. Reson. **188**, 285 (2007).
[10] M. E. Komlosh, F. Horkay, R. Z. Freidlin, U. Nevo, Y. Assaf, and P. J. Basser, J. Magn. Reson. **189**, 38 (2007) (http://dx.doi.org/10.1016/j.jmr.2007.07.003).
[11] S. Stapf, R. A. Damion, and K. J. Packer, J. Magn. Reson. **137**, 316 (1999).
[12] P. T. Callaghan and I. Furó, J. Chem. Phys. **120**, 4032 (2004) (http://dx.doi.org/10.1063/1.1642604).
[13] Y. Qiao, P. Galvosas, and P. T. Callaghan, Biophys. J. **89**, 2899 (2005) (http://dx.doi.org/10.1529/biophysj.105.064709).
[14] P. L. Hubbard, K. M. McGrath, and P. T. Callaghan, Langmuir **21**, 4340 (2005).
[15] P. L. Hubbard, K. M. McGrath, and P. T. Callaghan, Langmuir **22**, 3999 (2006) (http://dx.doi.org/10.1021/la052998n).
[16] P. L. Hubbard, K. M. McGrath, and P. T. Callaghan, J. Phys. Chem. B **110**, 20781 (2006) (http://dx.doi.org/10.1021/jp0601872).
[17] M. A. Koch and J. Finsterbusch, Proceedings of the International Society for Magnetic Resonance in Medicine 2005, Vol. 13, p. 840.
[18] M. A. Koch and J. Finsterbusch, Proceedings of the International Society for magnetic Resonance in Medicine 2006, Vol. 14, p. 1631.
[19] C. H. Ziener, T. Weber, W. R. Bauer, and P. M. Jakob, Proceedings of the International Society for Magnetic Resonance in Medicine 2007, Vol. 15, p. 13.
[20] P. T. Callaghan, A. Coy, D. MacGowan, K. J. Packer, and F. O. Zelaya, Nature (London) **351**, 467 (1991).
[21] P. T. Callaghan, *Principles of Nuclear Magnetic Resonance Microscopy* (Clarendon, Oxford, 1991).
[22] P. T. Callaghan, J. Magn. Reson. **129**, 74 (1997).
[23] C. H. Neuman, J. Chem. Phys. **60**, 4508 (1974).
[24] J. S. Murday and R. M. Cotts, J. Chem. Phys. **48**, 4938 (1968).
[25] P. J. Basser, J. Mattiello, and D. LeBihan, Biophys. J. **66**, 259 (1994).
[26] E. Özarslan and T. H. Mareci, Magn. Reson. Med. **50**, 955 (2003).
[27] E. Özarslan, T. M. Shepherd, B. C. Vemuri, S. J. Blackband, and T. H. Mareci, Neuroimage **31**, 1086 (2006).
[28] A. L. Sukstanskii, J. J. H. Ackerman, and D. A. Yablonskiy, Magn. Reson. Med. **50**, 735 (2003).
[29] E. Özarslan, U. Nevo, and P. J. Basser, Biophys. J. **94**, 2809 (2008) (http://dx.doi.org/10.1529/biophysj.107.124081).
[30] E. Özarslan, P. J. Basser, T. M. Shepherd, P. E. Thelwall, B. C. Vemuri, and S. J. Blackband, J. Magn. Reson. **183**, 315 (2006).
[31] A. Caprihan, L. Z. Wang, and E. Fukushima, J. Magn. Reson., Ser. A **118**, 94 (1996).
[32] S. L. Codd and P. T. Callaghan, J. Magn. Reson. **137**, 358 (1999).